Type XII collagen regulates osteoblast polarity and communication during bone formation

Yayoi Izu,[1] Mei Sun,[1] Daniela Zwolanek,[2] Guido Veit,[2] Valerie Williams,[4] Byeong Cha,[1] Karl J. Jepsen,[4] Manuel Koch,[2,3] and David E. Birk[1]

[1]Department of Pathology and Cell Biology, College of Medicine, University of South Florida, Tampa, FL 33612
[2]Institute for Oral and Musculoskeletal Biology, Center for Biochemistry and [3]Department of Dermatology, Center for Molecular Medicine Cologne, University of Cologne, D-50931 Cologne, Germany
[4]Leni and Peter W. May Department of Orthopaedics, Mount Sinai School of Medicine, New York, NY 10029

Differentiated osteoblasts are polarized in regions of bone deposition, demonstrate extensive cell interaction and communication, and are responsible for bone formation and quality. Type XII collagen is a fibril-associated collagen with interrupted triple helices and has been implicated in the osteoblast response to mechanical forces. Type XII collagen is expressed by osteoblasts and localizes to areas of bone formation. A transgenic mouse null for type XII collagen exhibits skeletal abnormalities including shorter, more slender long bones with decreased mechanical strength as well as altered vertebrae structure compared with wild-type mice. *Col12a*$^{-/-}$ osteoblasts have decreased bone matrix deposition with delayed maturation indicated by decreased bone matrix protein expression. Compared with controls, *Col12a*$^{-/-}$ osteoblasts are disorganized and less polarized with disrupted cell–cell interactions, decreased connexin43 expression, and impaired gap junction function. The data demonstrate important regulatory roles for type XII collagen in osteoblast differentiation and bone matrix formation.

Introduction

Osteoblast differentiation and maturation are crucial events in the formation of new bone and determination of bone quality (Nakashima et al., 2002; Yoshida et al., 2002; Komori, 2010). Bone formation begins with the differentiation of osteoblasts from pluripotent mesenchymal cells. The progenitors migrate to the sites of bone matrix deposition and differentiate into fully functional, bone matrix–producing osteoblasts (Imai et al., 1998). These events are regulated by the expression of runt-related gene 2 (*Runx2*, also known as *Cbfa1*) and sp7 transcription factor (*Sp7*, also known as osterix) and by canonical Wnt signaling followed by the secretion of specific bone matrix proteins such as type I collagen (*Col1a1*), secreted phosphoprotein1 (*Spp1*, also known as osteopontin), integrin-binding sialoprotein (*Ibsp*), and bone γ-carboxyglutamate protein (*Bglap*, also known as osteocalcin; Harada and Rodan, 2003; Koga et al., 2005). In addition to these changes in gene expression and matrix protein secretion, the mature osteoblasts become aligned along regions of bone deposition with an epithelioid arrangement. The mature, terminally differentiated osteoblasts are highly polarized relative to the site of bone matrix deposition (Ilvesaro et al., 1999; Nakashima et al., 2002; Stains et al., 2002). These features are common to periosteal and endosteal bone and both long and flat bones. Therefore, the alignment, polarization, and interaction of osteoblasts are important events necessary for production of a functional bone matrix.

Cell motility, communication, and shape are controlled via the local microenvironment where the extracellular matrix provides a substrate for cell anchorage, stores and presents growth factors or cytokines, and serves as a tissue scaffold (Rozario and DeSimone, 2010). The extracellular matrix interacts with the intracellular actin cytoskeleton via transmembrane proteins that affect cytoskeletal organization, cell motility and polarity, proliferation, and survival (Berthiaume et al., 1996; Geiger et al., 2001; Théry et al., 2005; Parsons et al., 2010; Kim et al., 2011). Thus, extracellular matrix–transmembrane protein–cytoskeleton

Correspondence to David E. Birk: dbirk@health.usf.edu

Y. Izu's present address is Dept. of Microbiology and Immunology, Penn State Milton S. Hershey College of Medicine, Hershey, PA 17033.

Abbreviations used in this paper: CT, computed tomography; FACIT, fibril-associated collagen with interrupted triple helices; HA, hydroxyapatite; H&E, hematoxylin and eosin; HU, Hounsfield unit; shRNA, short hairpin RNA; TMDn, tissue mineral density; TRAP, tartrate resistance acid phosphatase.

The Rockefeller University Press $30.00
J. Cell Biol. Vol. 193 No. 6 1115–1130
www.jcb.org/cgi/doi/10.1083/jcb.201010010

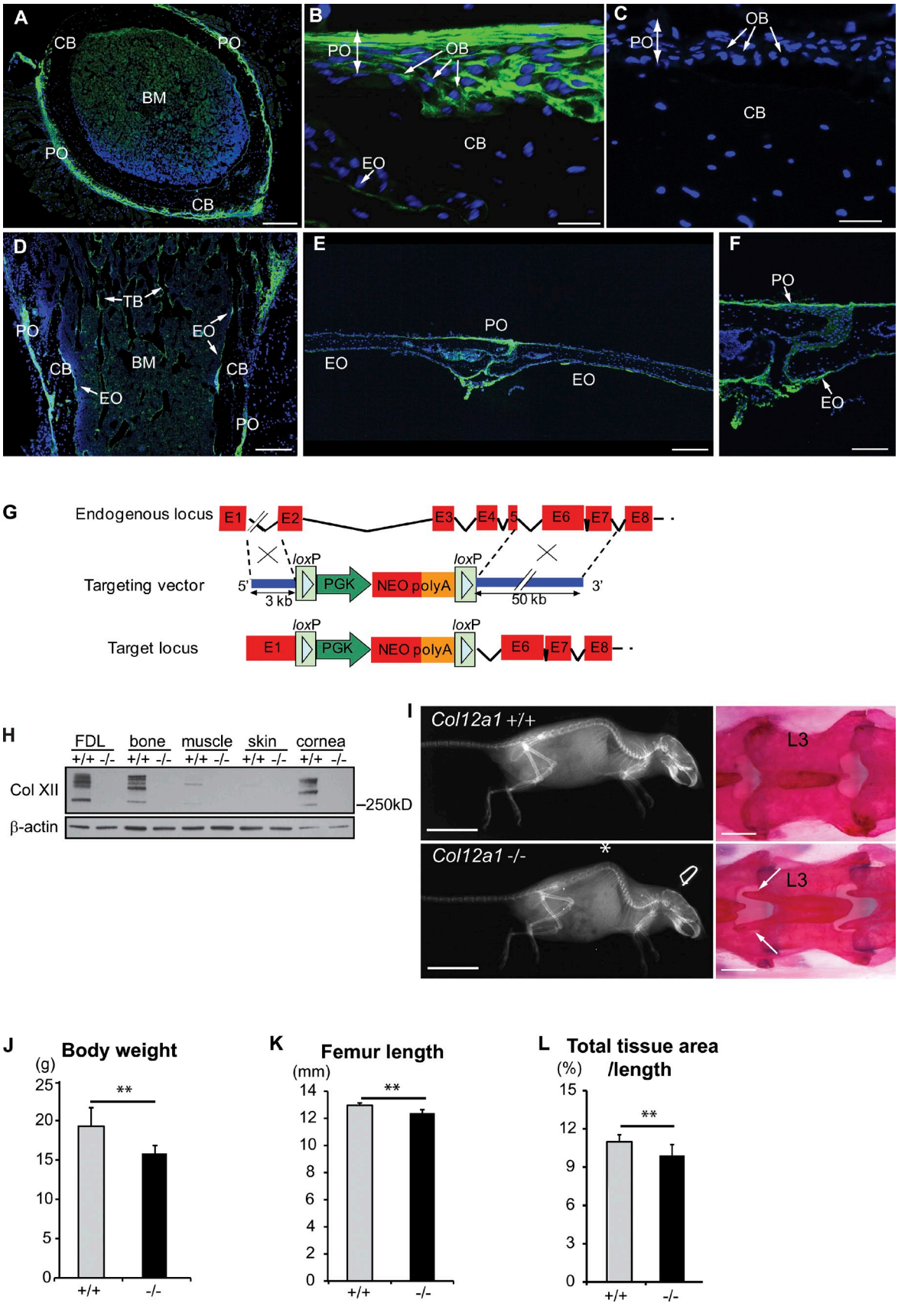

Figure 1. **Involvement of type XII collagen in bone formation.** (A–F) Type XII collagen is localized to bone-forming regions. Reactivity for type XII collagen is localized to the periosteum (PO), endosteum (EO), and trabecular bone (TB). Immunofluorescence analysis of the mid-diaphysis in cross (A and B) and longitudinal (D) sections of the femur and calvaria (E and F) from P30 wild type (*Col12a1*$^{+/+}$) and the mid-diaphysis in cross sections of the femur in type XII

interactions are important in the regulation of osteoblasts during bone formation. Integrins were shown to regulate osteoblast polarity and bone matrix deposition using mice expressing a dominant-negative truncated integrin β1 subunit (Zimmerman et al., 2000; Dobrowolski et al., 2008). In addition, extracellular matrix proteins, such as fibronectin (Globus et al., 1998) and osteopontin (Denhardt et al., 2001), are involved in osteoblast apoptosis and survival. Furthermore, the extracellular matrix is an important modulator of cell polarity and communication (Berthiaume et al., 1996; Geiger et al., 2001; Théry et al., 2005). However, the regulatory roles of the extracellular matrix in osteoblast organization, polarity, and communication during bone formation remain to be elucidated.

Type XII collagen is a member of the fibril-associated collagens with interrupted triple helices (FACITs) subfamily. FACITs are associated with striated fibrils assembled from fibrillar collagens such as type I collagen. In addition, they function at tissue interfaces, sites of cell-matrix communication (Wessel et al., 1997; Bader et al., 2009). Type XII collagen is a homotrimer of α1 chains and has three noncollagenous domains (NC1, NC2, and NC3) with two collagenous domains (COL1 and COL2). Two major splice variants with a molecular mass difference of 100 kD are generally coexpressed; however, the smaller form is predominant. The large splice variant contains sulfated glycosaminoglycans and is therefore also a proteoglycan. Although the functions of type XII collagen are not fully defined, evidence suggests that type XII collagen is a stress response molecule directly influenced by stretch and shear stress. It was reported that the *Col12a1* gene could be directly stimulated by mechanical forces in fibroblasts (Nishiyama et al., 1994; Flück et al., 2003) and endothelial cells (Jin et al., 2003) as well as osteoblasts (Arai et al., 2008). The mechanical strain response element is conserved in the first intron of the *Col12a1* gene in chicken, human (Chiquet et al., 1998), and mice (Arai et al., 2008).

Bone development and turnover/reorganization are influenced by mechanical stresses. Type XII collagen mRNA expression has been demonstrated in the periosteum, a site of active bone formation (Böhme et al., 1995). This suggests involvement of type XII collagen in the regulation of osteoblasts, including differentiation and maturation, alignment, polarization, and cell interactions. However, these potential regulatory roles of type XII collagen have not been defined. In this study, type XII collagen is demonstrated to be involved in the regulation of bone formation. Type XII collagen–null mice have fragile bones with a disorganized collagen fiber arrangement, decreased expression of bone matrix proteins, and decreased bone-forming activity associated with delayed terminal differentiation. These results are supported by morphological analysis demonstrating less organized and less polarized osteoblasts in vivo in the absence of type XII collagen. In addition, type XII collagen deficiency altered cell–cell interaction in osteoblasts and their derivatives and impaired gap junction communication through connexin43 (Cx43). Therefore, we hypothesize that type XII collagen regulates osteoblast organization and polarity as well as osteoblast–osteoblast and osteoblast–osteocyte communication required for normal bone deposition and the maintenance of bone quality and strength.

Results

Altered bone formation in type XII collagen–null mice

Type XII collagen was localized in bone-forming regions of wild-type mice by immunofluorescence analysis. Immunoreactivity for type XII collagen was detected in cortical and trabecular bone from femur and calvaria (Fig. 1, A–F). Type XII collagen was localized to the periosteum of the femurs from postnatal day 30 (P30) mice. The reactivity for type XII collagen was stable during development and growth (P1–P30). These results indicate that type XII collagen is localized to the areas where osteoblasts actively secrete bone matrix, and its expression is stable compared with the other skeletal tissues such as tendon and muscle (unpublished data). In addition, quantitative real-time PCR and Western blotting analysis revealed that osteoblasts express type XII collagen (Fig. 1 H; Arai et al., 2008). These data support a regulatory role for type XII collagen in bone formation by osteoblasts.

To analyze the regulatory role of type XII collagen in bone formation, *Col12a1*-null mice (*Col12a1*$^{-/-}$) were generated by the targeted deletion of exons 2–5 (Fig. 1 G). Type XII collagen expression was completely absent in this mouse model (Fig. 1 H). The *Col12a1*$^{-/-}$ mice demonstrated skeletal abnormalities (Fig. 1 I). They developed kyphosis with abnormally curved spines when compared with wild-type mice using x-ray analysis. An abnormality in vertebrae was present as double spinous processes. In addition, the *Col12a1*$^{-/-}$ mice exhibited a smaller stature indicated by a significant reduction in body weight compared with wild-type mice at age P30 (Fig. 1 J). The femurs of type XII collagen–null versus wild-type control mice were analyzed using 3D micro-computed tomography (CT; Fig. 1, K and L). These data indicate significantly shorter femur lengths and a significant reduction in the percentage of total tissue area/bone length, i.e., more slender bones when normalized

collagen–null (*Col12a1*$^{-/-}$) mice (C). Green, anti–type XII collagen; blue, nuclei reactive with DAPI; CB, cortical bone; BM, bone marrow; OB, osteoblast. (G) A schematic representation of the wild-type *Col12a1* exons 1–8 and target locus to create type XII collagen–null mice. After homologous recombination, the exon 2–5 locus was replaced by the selection cassette that includes the phosphoglycerolkinase (PGK) neomycin-polyadenylation (NEO polyA) signal. (H) Analysis of type XII collagen expression in tissues from wild-type and *Col12a1*$^{-/-}$ mice by immunoblotting. FDL, flexor digitorum longus. (I) X-ray and skeletal staining with alizarin red of 5-mo-old *Col12a1*$^{+/+}$ and *Col12a1*$^{-/-}$ mice. *Col12a1*$^{-/-}$ mice demonstrated kyphosis (asterisk) in the x-ray image. Abnormal double spinous processes (arrows) were present in the vertebral column of *Col12a1*$^{-/-}$ mice visualized by skeletal staining. L3, third lumbar. (J–L) Body weight, femur length, and percentage of tissue area/length were measured in P30 wild-type (control; $n = 9$) and type XII collagen–null ($n = 10$) mice. (J) Body weight is decreased in *Col12a1*$^{-/-}$ mice. (K) *Col12a1*$^{-/-}$ mice have shorter femurs compared with wild-type mice when normalized to body weight. (L) The percentage of tissue area/length normalized to body weight revealed that *Col12a*$^{-/-}$ mice have more slender femurs compared with wild-type controls. **, $P < 0.01$. Error bars are mean ± SD. Bars: (A, D, and E) 25 µm; (B, C, and F) 250 µm; (I, left) 2 cm; (I, right) 1 mm.

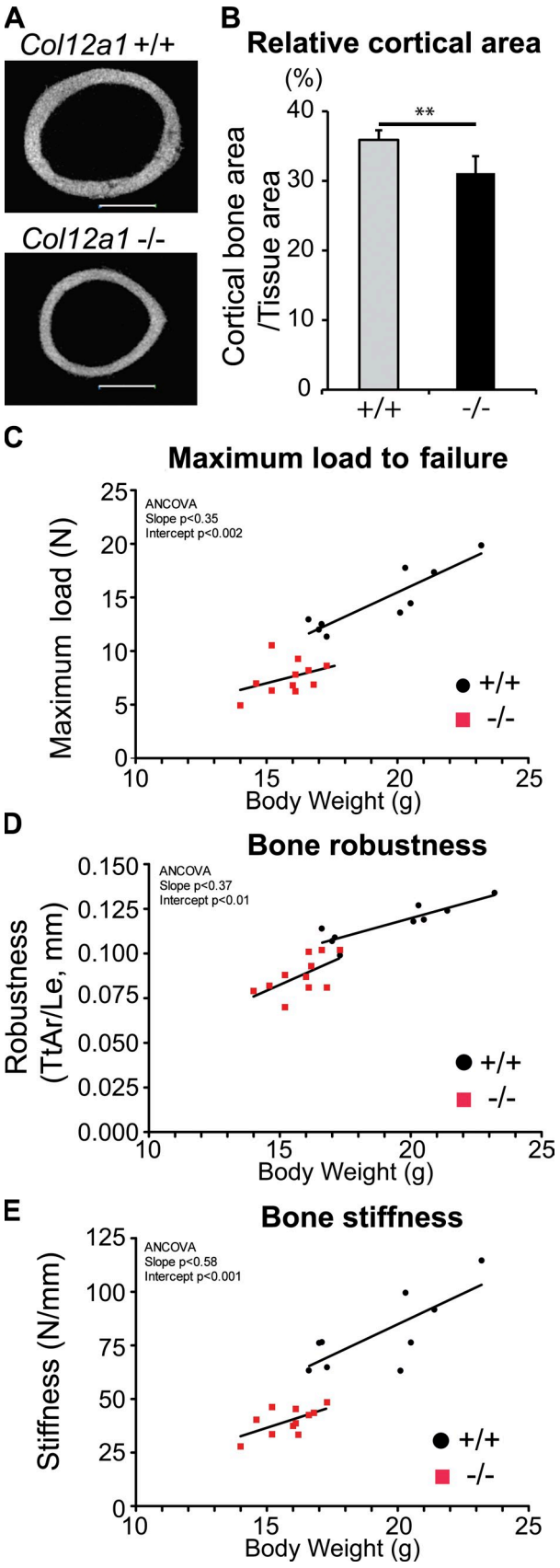

Figure 2. **Reduction of cortical bone mass and mechanical properties in *Col12a1*$^{-/-}$ long bones.** (A) *Col12a1*$^{-/-}$ mice have smaller diameters and less/thinner cortical bone compared with wild-type controls. 3D micro-CT images from the midshaft of a femur from P30 *Col12a1*$^{+/+}$ and *Col12a1*$^{-/-}$ mice. Bars, 0.5 mm. (B) Relative cortical area is significantly decreased in *Col12a1*$^{-/-}$ femurs. The relative cortical area was measured by 3D micro-CT analysis as the percentage of mineralized cortical bone area/mineralized tissue bone area normalized to body weight in P30 *Col12a1*$^{+/+}$ (n = 9) and *Col12a1*$^{-/-}$ (n = 10) mice. **, P < 0.01. Error bars are mean ± SD. (C–E) The biomechanical properties of the *Col12a1*$^{-/-}$ femurs were significantly reduced when compared with wild-type controls. Maximum to load failure (C), bone robustness (D), and bone stiffness (E) were measured in femurs of both *Col12a1*$^{+/+}$ (n = 9) and *Col12a1*$^{-/-}$ (n = 10) P30 mice by loading to failure in four-point bending at 0.05 mm/s and were normalized to body weight. Maximum load to failure, bone robustness, and bone stiffness are significantly decreased in *Col12a1*$^{-/-}$ mice. TtAr/Le, total cross-sectional area/bone length; N/mm, Newtons per millimeter. P < 0.01.

to body weight. Therefore, the presence of type XII collagen in bone-forming regions and abnormal skeletal development in the absence of type XII collagen support an essential role for type XII collagen in the regulation of bone formation.

Col12a1$^{-/-}$ mice have decreased cortical bone mass and weaker, more fragile bones

The influence of type XII collagen on the structure of long bones and their mechanical properties was analyzed in *Col12a1*$^{-/-}$ and wild-type mice (Fig. 2). The femurs from P30 *Col12a1*$^{-/-}$ mice had smaller diameters and proportionally less cortical bone mass compared with wild-type mice when analyzed using 3D micro-CT. Statistical analysis of the micro-CT data normalized to body weight demonstrated an ∼10% reduction in cortical bone thickness compared with wild-type controls. In addition, the mechanical properties analyzed using a four-point bending procedure were significantly reduced in the type XII collagen–null femurs normalized for body weight. The maximum load to failure, bone robustness, and bone stiffness were all significantly decreased in *Col12a1*$^{-/-}$ compared with wild-type mice. These data indicate that bones from *Col12a1*$^{-/-}$ mice were not just smaller and thinner but also had decreased bone quality relative to body size compared with wild-type controls.

Delayed or decreased bone matrix deposition in *Col12a1*$^{-/-}$ osteoblasts

To analyze bone deposition, in vitro mineralized bone nodule formation analyses were conducted using bone marrow cells from P30 wild-type and *Col12a1*$^{-/-}$ mice in osteogenic medium and analyzed after 14, 21, and 28 d in culture (Fig. 3 A). Mineralized nodules were present in wild-type osteoblasts after 14 d, whereas nodules were virtually absent from cultures of *Col12a1*$^{-/-}$ osteoblasts under the same conditions. At day 21, nodules were formed in cultures of both genotypes, but the mineralized nodule area in the *Col12a1*$^{-/-}$ cultures was significantly smaller than in wild-type cultures. At 28 d in culture, nodule formation was not as robust in *Col12a1*$^{-/-}$ compared with wild-type osteoblasts. However, the difference between osteoblasts from the different genotypes was no longer significant, suggesting a delayed bone deposition and/or decreased bone-forming activity in the absence of type XII collagen.

The in vitro bone formation data were confirmed in vivo using calcein double labeling in P30 wild-type and *Col12a1*$^{-/-}$

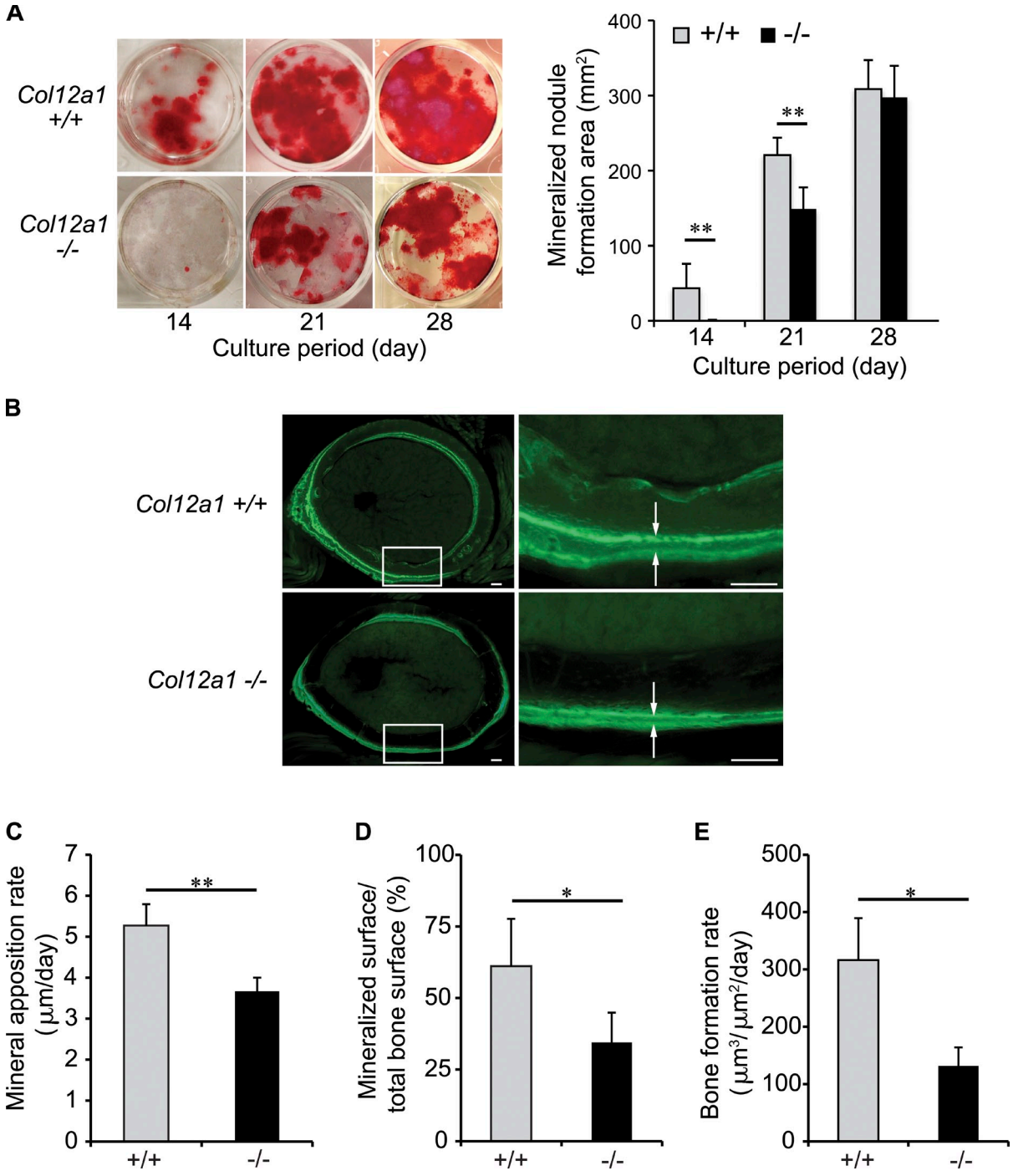

Figure 3. **Decreased bone formation in type XII collagen–null mice.** (A) Decreased mineralized nodule formation was observed in bone marrow cells derived from P30 *Col12a1*$^{-/-}$ mice (n = 6) compared with wild-type controls (n = 5). Cells were cultured in osteogenic medium for 14, 21, and 28 d. Mineralized nodules represented by alizarin red staining are detected in wild-type cells after 14 d in culture, whereas nodules are virtually absent from *Col12a1*$^{-/-}$ cells under the same conditions. At day 21, although nodules are formed in the *Col12a1*$^{-/-}$ bone marrow cells, the nodule area is smaller than that in wild-type cultures. Similar nodule areas are detected at 28 d in culture. The mineralized nodule area is significantly decreased in *Col12a1*$^{-/-}$ bone marrow cells at both day 14 and 21 in culture compared with wild-type controls. At day 28, the areas are comparable, indicating a delay in the absence of type XII collagen. (B–E) Bone morphometry in the periosteum of cross sections of tibia from P30 *Col12a1*$^{-/-}$ (n = 5) and wild-type control (n = 4) mice was conducted using calcein double labeling. (B) Calcein label is detected as double lines (arrows). The boxed areas on the left are shown at higher magnification on the right. The distance between labels is decreased in *Col12a1*$^{-/-}$ bone compared with wild-type control. (C) Mineral apposition rate is reduced ~30% in *Col12a1*$^{-/-}$ mice compared with wild-type controls. (D and E) The type XII collagen–null bones have ~40% of the percentage of mineralized bone surface/total bone surface (D) and ~50% of the bone formation rate (E) in *Col12a1*$^{-/-}$ mice compared with wild-type controls. All of the differences are significant. *, $P < 0.05$; **, $P < 0.01$. Error bars are mean ± SD. Bars, 100 μm.

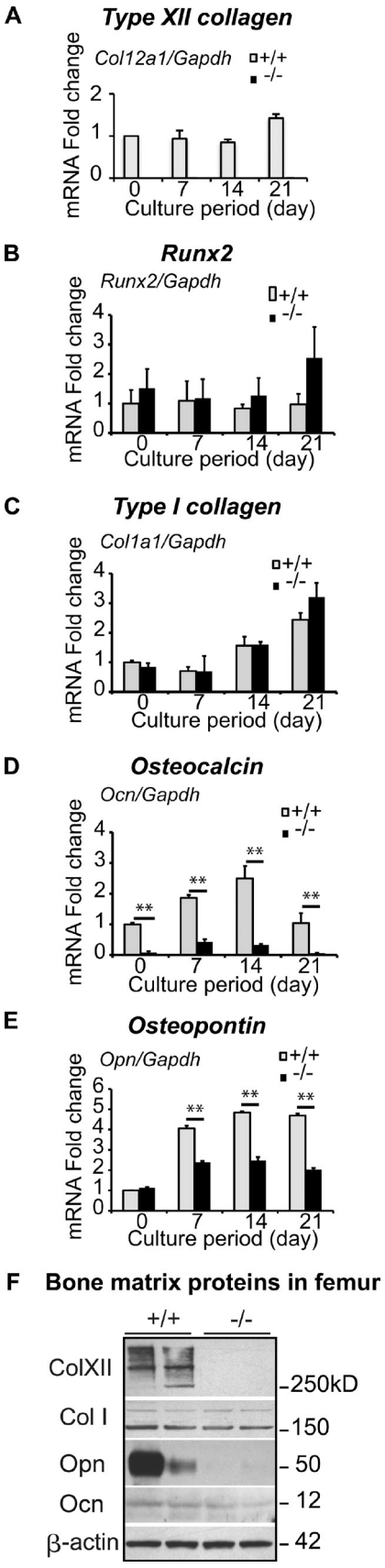

Figure 4. **Delayed terminal differentiation in type XII collagen–null osteoblasts.** (A–E) Primary osteoblasts were derived from neonatal calvaria of *Col12a1*$^{+/+}$ and *Col12a1*$^{-/-}$ mice and cultured in osteogenic medium. The cells are harvested after 0, 7, 14, and 21 d in culture and used for quantitative real-time PCR analysis. Each group represents the mean of triplicate determinations. mRNA was normalized to *Gapdh* expression. (A) Type XII collagen mRNA expression is stable during osteoblast development. (B and C) Similar expression patterns are detected in mRNA expressions of *Runx2* (B) and *type I collagen* (C) in *Col12a1*$^{+/+}$ and *Col12a1*$^{-/-}$ osteoblasts. (D and E) The expression of osteocalcin (*Ocn*; D) and osteopontin (*Opn*; E), which are terminal osteoblast differentiation markers, is significantly decreased in *Col12a1*$^{-/-}$ osteoblasts as compared with wild-type controls. **, $P < 0.01$. Error bars are mean ± SD. (F) Immunoblot analysis of P30 femurs from *Col12a1*$^{+/+}$ ($n = 2$) and *Col12a1*$^{-/-}$ ($n = 3$) mice was performed to validate the in vitro data. Opn and Ocn expression is decreased, whereas type I expression is stable in *Col12a1*$^{-/-}$ femurs compared with the mRNA data.

mice (Fig. 3, B–E). Nondecalcified cross sections demonstrated decreased calcein-labeling intervals in the periosteal region of *Col12a1*$^{-/-}$ bone compared with wild-type controls. This interval in the endosteum is comparable in both genotypes (unpublished data). Based on this calcein double labeling, the mineral apposition rate, percentage of mineralized surface/total bone surface, and bone formation rate were analyzed. All indices were significantly decreased in *Col12a1*$^{-/-}$ mice compared with wild-type controls. These data indicate that the absence of type XII collagen was associated with decreased bone formation in osteoblasts.

The potential involvement of bone resorption versus decreased bone formation in the absence of type XII collagen was investigated. The C-terminal telopeptide of collagen I (CTx), a biochemical marker of bone resorption, was analyzed, and there was no significant difference in serum levels between *Col12a1*$^{-/-}$ and wild-type control mice at age P30 (Fig. S1 A). The expression of bone resorption markers, such as *tartrate resistance acid phosphatase* (*Trap*), *nuclear factor of activated T cells cytoplasmic 1* (*Nfatc1*), *receptor activator of NFκ-B* (*Rank*), and *rank ligand* (*Rankl*), were analyzed from whole femurs by real-time PCR, and no significant differences between *Col12a1*$^{-/-}$ and wild-type mice were observed (Fig. S1 B). Finally, osteoclast number per bone surface and osteoclast surface per bone surface (Fig. S1 C) were also comparable in *Col12a1*$^{-/-}$ and wild-type controls as observed by Trap staining. These data indicate that the decreased bone mass in *Col12a1*$^{-/-}$ mice was not a result of increased osteoclast resorption but resulted from abnormal osteoblast bone formation.

Type XII collagen is involved in the regulation of osteoblast terminal differentiation

The delayed/decreased mineralized nodule formation in osteoblast cultures from type XII collagen–null mice suggests altered or delayed osteoblast differentiation (Fig. 4). To investigate the involvement of the type XII collagen in osteoblast differentiation, the expression of osteoblast differentiation markers was used. *Runx2* was used as an early stage marker, type I collagen (*Col1a1*) was used as a middle-stage marker, and osteocalcin (*Ocn*) and osteopontin (*Opn*) were used as late-stage markers. Primary osteoblasts from neonatal calvaria of both genotypes were cultured in osteogenic medium and analyzed after 0, 7, 14, and 21 d using quantitative real-time PCR.

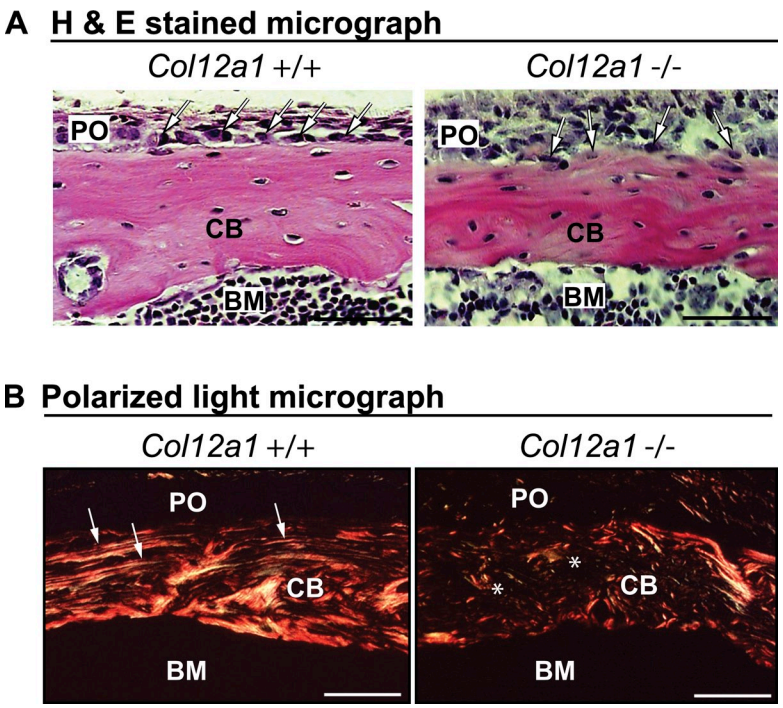

Figure 5. **Disorganized bone matrix collagen arrangement in type XII collagen–null mice.** (A) Osteoblast morphology was analyzed in cross sections of the diaphysis from femurs of P30 *Col12a1*$^{+/+}$ and *Col12a1*$^{-/-}$ mice with H&E staining. Osteoblasts in wild-type bone are localized on the surface of cortical bone (CB), where they are aligned and well organized in an epithelioid manner (arrows). In contrast, *Col12a1*$^{-/-}$ osteoblasts (arrows) are poorly aligned and crowded in the periosteum (PO) with a disorganized arrangement associated with the surface of cortical bone. BM, bone marrow. (B) Collagen organization was analyzed in cross sections of the diaphysis from femurs of P14 *Col12a1*$^{+/+}$ and *Col12a1*$^{-/-}$ mice. To analyze collagen organization, Sirius red staining with polarized light microscopy was performed. Collagen fibers (arrows) are arranged in parallel and are well organized in the wild-type cortical bone matrix, whereas birefringence is sparse in *Col12a1*$^{-/-}$ mice, indicating smaller and/or less organized collagen fibers (asterisks) in the cortical bone. Bars, 50 µm.

Comparable expression patterns were detected for *Runx2* and type I collagen in wild-type and *Col12a1*$^{-/-}$ osteoblasts (Fig. 4, B and C). In contrast, expression of osteocalcin and osteopontin, markers for late-stage osteoblast development, was significantly decreased in *Col12a1*$^{-/-}$ osteoblasts compared with wild-type controls (Fig. 4, D and E). The mRNA expression data were validated using immunoblot analyses of type I collagen, osteocalcin, and osteopontin from P30 femurs (Fig. 4 F). There was no difference in type I collagen in the two genotypes; however, both osteopontin and osteocalcin were decreased in the type XII collagen–null femurs. This was analyzed further using short hairpin RNA (shRNA) for a functional *Col12a1* gene knockdown in murine preosteoblastic cells (MC3T3-E1). Lentivirus transduction with the specific shRNA demonstrated an ∼40% reduction of *Col12a1* mRNA expression (Fig. S2, A–D). In this system, the *Col12a1* knockdown had no effect on *Runx2* or type I collagen mRNA expression. However, a reduction in *Ocn* mRNA expression was observed (Fig. S2, B–D). Protein levels for type I collagen were unaffected with both osteopontin and osteocalcin showing reduced protein expression in the type XII collagen knockdown cultures (Fig. S2 E). These data are comparable with that obtained from the type XII collagen–null mice. The comparable expression patterns observed in both systems fully support a role for type XII collagen in the regulation of osteoblast terminal differentiation.

Col12a1$^{-/-}$ bone exhibits altered collagen fiber organization and disorganization of osteoblasts/osteocytes

The in vivo phenotype of femurs from *Col12a1*$^{-/-}$ mice was analyzed for bone matrix organization as well as osteoblast/osteocyte organization. Osteoblasts in wild-type bone were localized on the surface of cortical bone, where they were aligned and well organized in an epithelioid manner when analyzed in hematoxylin and eosin (H&E)–stained sections (Fig. 5 A). In contrast, *Col12a1*$^{-/-}$ osteoblasts were poorly aligned, with a disorganized arrangement relative to the surface of cortical bone (Fig. 5 A). Collagen fiber organization was analyzed in cross sections of the diaphysis of femurs from P14 wild-type and *Col12a1*$^{-/-}$ mice using Sirius red staining with polarized light microscopy (Fig. 5 B). Large birefringent collagen fibers were arranged in parallel and were well organized in the wild-type cortical bone matrix. In contrast, birefringence was sparse and disorganized in *Col12a1*$^{-/-}$ bone matrix, indicating that collagen fibers were smaller and/or less organized in *Col12a1*$^{-/-}$ cortical bone compared with controls. These results indicate that type XII collagen is involved in determining osteoblast organization and normal bone matrix quality.

To further analyze osteoblast organization and polarity along the bone deposition interface, osteoblasts in the periosteum were analyzed using confocal microscopy with nuclear, actin cytoskeletal, and Golgi markers (Fig. 6). Osteoblasts in wild-type bone were well organized in an epithelioid manner along the bone interface. These osteoblasts exhibited a well-organized circumferential actin cytoskeleton with a peripheral localization. In addition, the actin fibers were localized in osteoblast–osteocyte processes interacting in the bone matrix to create an extensive osteoblast–osteocyte network. Overall, the nuclear and Golgi markers were localized in a polarized manner, in which Golgi usually locate toward the cortical bone opposite the nuclei. In contrast, *Col12a1*$^{-/-}$ osteoblasts were poorly organized along the bone interface. The actin cytoskeleton was also poorly organized, composed of clumps of actin fibers showing random distribution around the cells. In addition, fewer osteoblast/osteocyte processes were observed in the bone matrix, indicating a less extensive osteoblast–osteocyte network than present in the wild-type bone. The nuclear and Golgi markers were not as polarized as in the control mice.

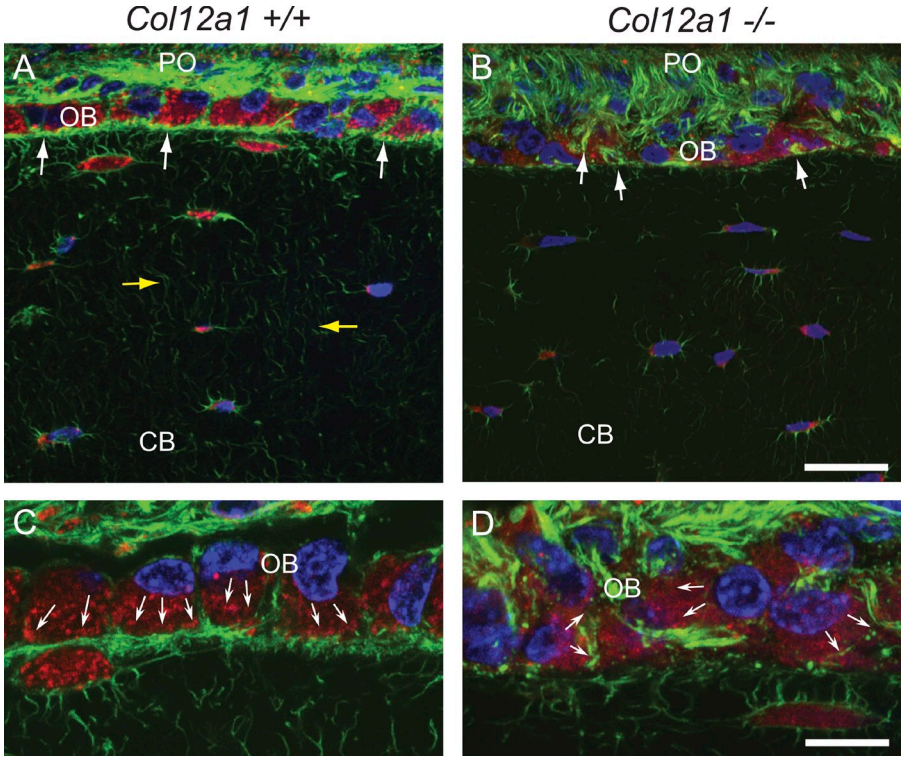

Figure 6. **Defective organization and polarization of osteoblasts in type XII collagen–null bone.** Osteoblast polarization was analyzed by the distribution of nucleus, Golgi apparatus, and F-actin staining with confocal fluorescence microscopy. (A) Wild-type osteoblasts (OB) in an epithelioid arrangement are well organized into a layer between the periosteum (PO) and cortical bone (CB), and F-actin fibers (green) are highly enriched in regions of the osteoblasts, which face the periosteum and cortical bone (white arrows). (B) In contrast, *Col12a1*$^{-/-}$ osteoblasts are not well organized between the periosteum and cortical bone, and F-actin fibers appear to form aggregates distributed randomly within osteoblasts (arrows). (C) Wild-type osteoblasts exhibit a polarized distribution of the Golgi apparatus (red) and the nucleus (blue). Most Golgi reactivity is localized toward the bone matrix (arrows), whereas the nuclei were positioned to the opposite side. (D) *Col12a1*$^{-/-}$ osteoblasts also fail to show a polarized distribution of Golgi and nucleus. It is noticeable that the F-actin fibers (yellow arrows) extend to the cortical bone matrix, establishing a network throughout the bone matrix in wild-type bone. This network is not as extensive in *Col12a1*$^{-/-}$ bone. Bars: (A and B) 20 µm; (C and D) 10 µm.

These data indicate a role for type XII collagen in the organization of osteoblasts into well-organized and polarized layers necessary for regulated bone matrix deposition.

Because *Col12a1*$^{-/-}$ osteoblasts showed a disorganized arrangement at the bone surface and a less extensive osteoblast–osteocyte network, a defect in osteoblast to osteocyte transition was hypothesized. To address this hypothesis, osteocyte density was analyzed as osteocyte number/100 µm^2 in H&E sections. A significant increase (~60%) in the number of osteocytes in *Col12a1*$^{-/-}$ compared with wild-type cortical bones was observed (Fig. S3). These data indicate that type XII collagen deficiency results in abnormal arrangement and polarization of osteoblast linage cells in the periosteum and suggests a dysfunctional, premature osteoblast to osteocyte transition.

Defects in osteoblast polarity and altered cell–cell interaction and/or communication in *Col12a1*$^{-/-}$ bones

To further analyze the morphological phenotype of osteoblasts and osteocytes of *Col12a1*$^{-/-}$ and wild-type mice, transmission EM was conducted during an active bone-forming period (P14; Fig. 7, A–C). The wild-type osteoblasts were attached to the surface of cortical bone and were aligned along the region of bone formation. In addition, the osteoblasts were well polarized relative to the bone matrix. In contrast, the *Col12a1*$^{-/-}$ osteoblasts were less organized and poorly polarized (Fig. 7 A). This was consistent with the data observed by confocal immunofluorescence microscopy. The analysis of adjacent osteoblasts in the periosteum revealed that wild-type osteoblasts had numerous processes that connected osteoblast–osteoblast and osteoblast–osteocyte. In contrast, *Col12a1*$^{-/-}$ osteoblasts had large intracellular spaces with fewer processes (Fig. 7, B and C). This was consistent with the disorganized actin cytoskeleton observed by confocal microscopy. This indicates altered cell–cell interaction and/or communication in the absence of type XII collagen in bone. Similar to the osteoblast phenotype, osteocytes had processes that interact with other osteocytes and/or toward the cortical bone surface connecting to other osteocytes or osteoblasts in wild-type bone. However, *Col12a1*$^{-/-}$ osteocytes had fewer and less developed processes (Fig. 7 D). This is consistent with the altered osteocyte number/distribution observed (Fig. 6, A and B; and Fig. S3). Thus, type XII collagen–null bones are associated with alterations in cell–cell interactions that may lead to altered cell–cell communication.

Type XII collagen mediates osteoblast–osteoblast communication via regulation of Cx43 expression

Based on the morphological findings that indicate altered cell–cell interaction, the expression of gap junction proteins and cell adhesion molecules was investigated to determine the relationship between type XII collagen and cell–cell communication. Gap junction proteins and cadherins are required for coordination of mechanical and chemical signal transduction in bone development and formation (Civitelli, 2008; Matsuo and Irie, 2008). A quantitative analysis of Cx43 and cadherin 2 and 11 (Cad2 and Cad11) was performed using primary osteoblasts after 0, 7, 14, and 21 d in culture (Fig. 8, A–E; and Fig. S4 A). *Cx43* mRNA expression was significantly decreased at each time point in *Col12a1*$^{-/-}$ osteoblast cultures versus wild-type control cultures. As expected, type XII collagen mRNA expression was stable (Fig. 4 A). Interestingly, the difference

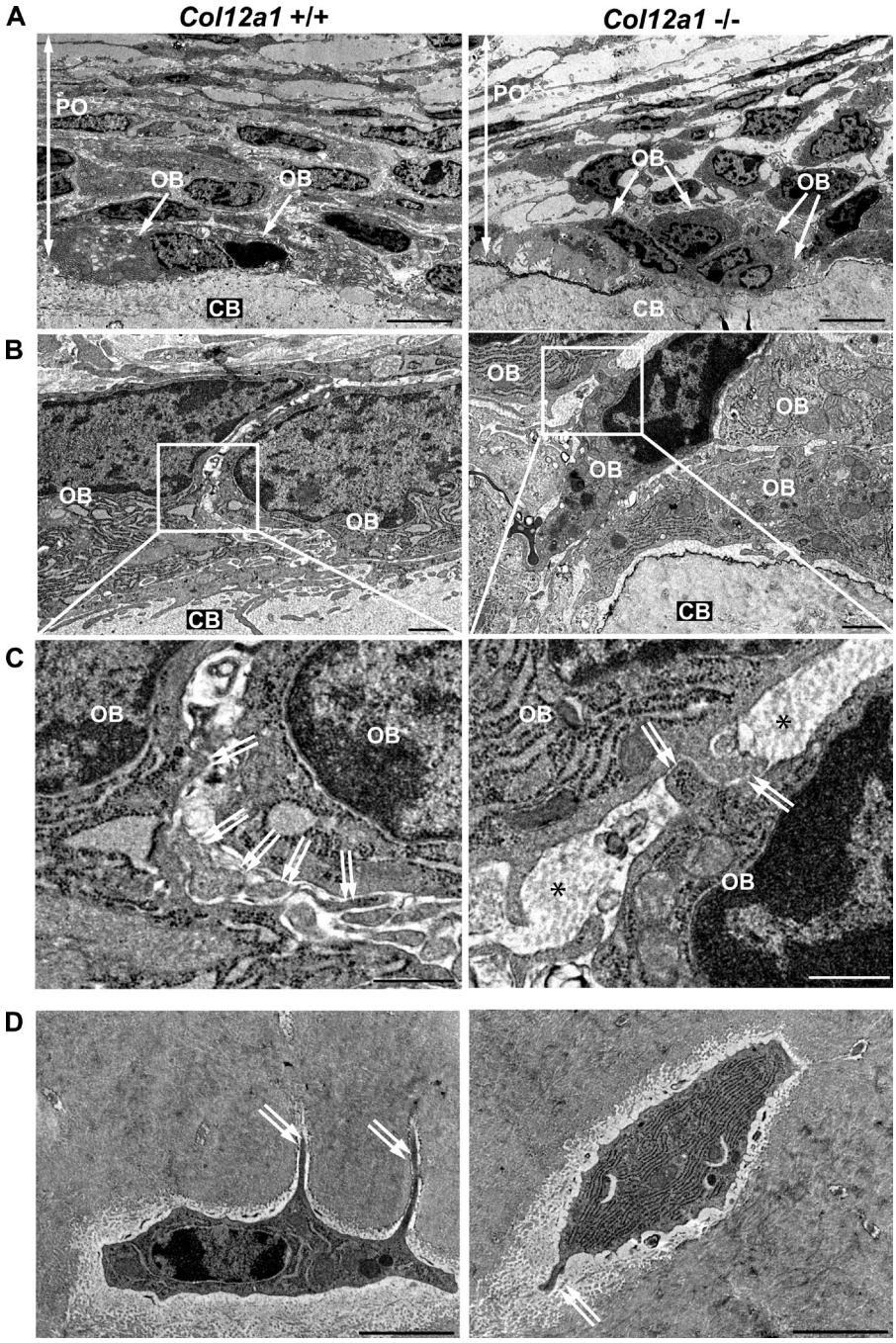

Figure 7. **Altered cell–cell interaction/communication in type XII collagen–null bone in vivo.** Analysis of cross sections from the diaphysis of femurs in P14 *Col12a1*$^{+/+}$ and *Col12a1*$^{-/-}$ mice using transmission EM. (A) Wild-type osteoblasts (OB) attached to the surface of cortical bone (CB) are elongated and polarized relative to the bone matrix. In contrast, *Col12a1*$^{-/-}$ osteoblasts (arrows) are disorganized and less polarized. PO, periosteum. (B and C) High magnification of adjacent osteoblasts in the periosteum. In wild-type bone, osteoblasts have numerous processes (double arrows) that connect osteoblast to osteoblast. *Col12a1*$^{-/-}$ osteoblasts have large intracellular spaces (asterisks) with fewer processes (double arrows). (D) Osteocyte within cortical bone matrix. Similar to the osteoblast phenotype, an osteocyte has processes (double arrows) that extend toward the cortical bone surface in wild-type bone connecting to other osteocytes or osteoblasts; however, *Col12a1*$^{-/-}$ osteocytes have fewer and less developed processes (double arrows). Bars: (A) 5 µm; (B) 1 µm; (C) 500 nm; (D) 2 µm.

between genotypes was detected only in early stage osteoblasts (0 and 7 d in culture) in *Cad11* expression but not in *Cad2* and *Cad11* expression in late-stage osteoblasts in *Col12a1*$^{-/-}$ cultures versus the wild-type controls. The mRNA expression was consistant with immunoblot analysis in primary osteoblasts (Fig. 8, D–F; and Fig. S4). The expression of Cx43 protein was decreased in *Col12a1*$^{-/-}$ primary osteoblasts as well as in *short hairpin Col12a1* (*shCol12a1*)–treated MC3T3-E1 cells with differentiation and P30 whole femurs, consistent with the mRNA expression results. Therefore, the absence of type XII collagen leads to decreased Cx43 expression at both mRNA and protein levels. Type XII collagen protein increased with osteoblast development. However, a relationship between the increase of type XII collagen and Cx43 expression was not detected in normal osteoblast development because Cx43 expression was stable in both mRNA and protein in cultured wild-type osteoblasts in osteogenic medium (Fig. 8 D). To investigate the possible interaction of type XII collagen and Cx43, coimmunoprecipitation assays were performed in wild-type primary osteoblasts and MC3T3-E1 cells cultured in osteogenic medium. Immunoprecipitation with anti–type XII collagen antibody did not pull down Cx43 and vice versa (unpublished data). These results suggest that the type XII collagen may indirectly regulate Cx43 expression during bone formation, perhaps by altering cell behavior during transition to the organized and polarized osteoblastic layer.

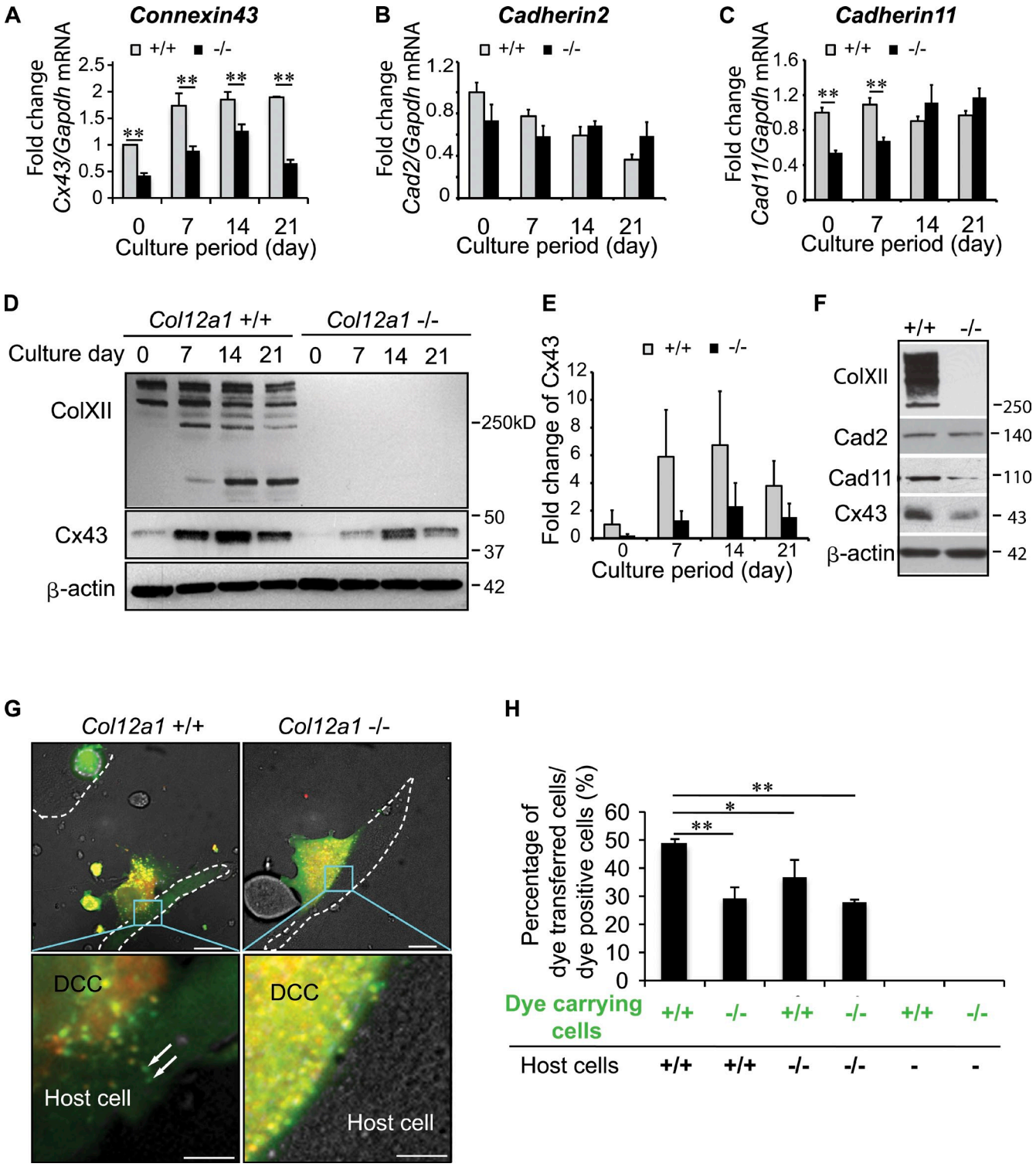

Figure 8. **Impaired cell–cell communications via gap junction associated with altered Cx43 expression in type XII collagen–null osteoblasts.** (A–C) Analysis of Cx43 (*Cx43*; A), Cad2 (*Cad2*; B), and Cad11 (*Cad11*; C) mRNA expression in cultures of primary osteoblasts by quantitative real-time PCR normalized to *Gapdh* expression. Each group represents the mean of triplicate determinations. (A) *Cx43* expression is significantly decreased at every time point in *Col12a1*$^{-/-}$ osteoblast cultures. (B) No significant difference between genotypes is detected in *Cad2* expression. (C) *Cad11* expression is decreased in early stages in *Col12a1*$^{-/-}$ osteoblast cultures but not in late stages. **, $P < 0.01$. (D) Immunoblot analysis of *Cx43* in cultures of primary osteoblasts. β-Actin is used as an internal control. (E) The relative band density of Cx43 normalized to β-actin. Each group represents the mean of triplicate determinations. Cx43 expression is decreased in *Col12a1*$^{-/-}$ osteoblasts. (F) Immunoblot analysis of Cx43, Cad2, and Cad11 in P30 femurs from *Col12a1*$^{+/+}$ ($n = 2$) and *Col12a1*$^{-/-}$ ($n = 3$) mice. Cx43 and Cad11 expression is decreased in *Col12a1*$^{-/-}$ femurs. Molecular mass is indicated in kilodaltons. (G) Dye coupling study in primary osteoblasts. Calcein AM– and Cell Tracker–labeled osteoblasts (DCC, dye-carrying cells) were seeded onto confluent osteoblasts (host cells) and analyzed by confocal microscopy. The dashed lines indicate the outline of host cells. High magnification of the site of dye-carrying wild-type osteoblasts (+/+) attaching to the wild-type host osteoblasts demonstrates transfer, i.e., the green dots (arrows) to the host cell. Although the *Col12a1*$^{-/-}$ osteoblast is attaching to the *Col12a1*$^{-/-}$ host cell, calcein dye stays within the donor cell (i.e., no transfer is observed). Bars: (top) 25 µm; (bottom) 10 µm.

Based on the decreased expression of Cx43 in type XII collagen–null osteoblasts, a dye coupling assay was used to clarify whether type XII collagen can regulate gap junction–mediated intercellular communication (Fig. 8, G and H; and Videos 1 and 2). Osteoblasts were labeled with calcein acetoxymethyl ester (AM) dye and seeded onto unlabeled confluent osteoblasts. Dye transfer was examined and quantitated using confocal microscopy. The wild-type dye-carrying osteoblasts continuously transferred dye to unlabeled osteoblasts (host cells) after the dye-carrying cells attached to the host. In contrast, in the majority of *Col12a1*$^{-/-}$ osteoblasts, the dye was not transferred and remained within the cells after attachment to *Col12a1*$^{-/-}$ host cells. The percentage of dye-transferred cells was significantly decreased when either dye-carrying or host cells are *Col12a1*$^{-/-}$. A reduction of ∼40% was observed compared with dye-carrying wild-type cells on wild-type host cells. A similar reduction in dye transfer was observed using *Col12a1* knockdown MC3T3-E1 cells (Fig. S5). These results indicate that type XII collagen deficiency impaired gap junction communication possibly through altered Cx43 expression.

These results indicate a critical role for type XII collagen in bone formation. The absence of type XII collagen resulted in decreased bone quality associated with altered osteoblast organization, decreased polarity, and altered bone matrix deposition. In addition, type XII collagen–null osteoblasts had altered cell–cell interactions that impaired gap junction communication and Cx43 expression.

Discussion

Cell shape and polarity are essential for cell proliferation, development, and function. This is regulated by extracellular matrix–transmembrane protein–cytoskeleton interactions (Geiger et al., 2001; Burgstaller et al., 2010; Kim et al., 2011). In bone formation, osteoblasts become highly polarized, align along the bone matrix, and develop intercellular interactions during maturation. However, the regulation of osteoblast shape and cell–cell interaction during maturation and bone formation remains unclear. Here, we demonstrate that type XII collagen regulates osteoblast differentiation and maturation, alignment, interaction, and polarization. The genetic deletion of type XII collagen results in abnormal osteoblast differentiation, decreased bone matrix deposition, and decreased bone quality. This is related to impaired terminal differentiation of osteoblasts.

Osteoblasts and osteocytes express several different integrins that connect the cytoskeleton with the extracellular matrix. The functional roles of integrins in osteoblast development and bone formation have been examined. Interestingly, less polarization of mature osteoblasts and impaired process formation in osteocytes were demonstrated using transgenic mice with a dominant-negative β1 integrin driven by the osteocalcin promoter, which is expressed only in mature osteoblasts and osteocytes (Zimmerman et al., 2000). These data are comparable with our current results, suggesting a potential type XII collagen–integrin regulatory interaction. Type XII collagen has an RGD (Arg-Gly-Asp) peptide sequence (Oh et al., 1992), which is a cell adhesion motif suggesting that type XII collagen may regulate osteoblast polarization via an RGD site interacting with a β1 integrin during maturation. However, other indirect interactions mediated by intermediary matrix molecules should also be considered. Type XII collagen also has a mechanical strain response element in the *Col12a1* gene (Arai et al., 2008), and evidence indicates an involvement of type XII collagen in the mechanical response. Cell shape, alignment, and organization are also regulated by mechanotransduction. Osteoblasts respond to cyclic mechanical bending, and osteoblast/osteocyte communication via gap junctions transmits mechanical signals (Duncan and Turner, 1995; Jiang et al., 2007; Shapiro, 2008) that result in osteoblast differentiation, growth, and bone matrix deposition. Therefore, type XII collagen may be expressed in response to mechanical forces and expressed at the osteoblast surface where it transduces the signal to the cytoskeleton through integrins, thereby stimulating osteoblast terminal differentiation in bone-forming regions.

Communication in mature osteoblasts and osteoblasts–osteocytes is controlled via gap junctions. Cx43 is the most abundant gap junction component in osteoblast cell coupling and the osteocyte network within the bone matrix. The functional disruption of *Cx43* causes delayed osteoblast differentiation with decreased expression of osteocalcin and delayed ossification in vivo (Lecanda et al., 2000; Civitelli, 2008; Dobrowolski et al., 2008). These data support our hypothesis that type XII collagen regulates cell–cell communication and mediates gap junction function. The function of type XII collagen in mediating cell shape changes and cell organization may regulate Cx43 expression and gap junction function. This is consistent with data indicating that the extracellular matrix, especially laminin, regulates connexin expression and functions through gap junctions in neural progenitor cells (Imbeault et al., 2009). In addition to a fibril-associated localization, type XII collagen is localized to basement membrane zones in many tissues (Wessel et al., 1997; Bader et al., 2009). Our dye coupling experiment revealed that gap junction communication was impaired in the absence of type XII collagen even when osteoblasts were in direct contact with each other. Moreover, Cx43 is involved in transmitting signals that induce bone formation in response to in vivo mechanical loading (Grimston et al., 2008). Our coimmunoprecipitation assays revealed no direct interaction in type XII collagen and Cx43. Thus, type XII collagen may regulate gap junction communication and Cx43 expression in osteoblast linage cells, but this may be an indirect regulation.

Alteration of cell shape and mobility also influences cell matrix production. Maintenance of bone quality is important

(H) The number of dye-transferred cells per total parachuted cells was determined in 10 random images acquired from each well (24-well plate), and 6 wells were used per experimental group. As compared with dye-carrying wild-type cells (+/+) on wild-type host cells, the percentage of dye-transferred cells is significantly decreased when either dye-carrying or host cells are *Col12a1*$^{-/-}$. A reduction of ∼40% is detected when compared with wild-type versus wild-type and *Col12a1*$^{-/-}$ versus *Col12a1*$^{-/-}$ cells. *, $P < 0.05$; **, $P < 0.01$. Error bars are mean ± SD.

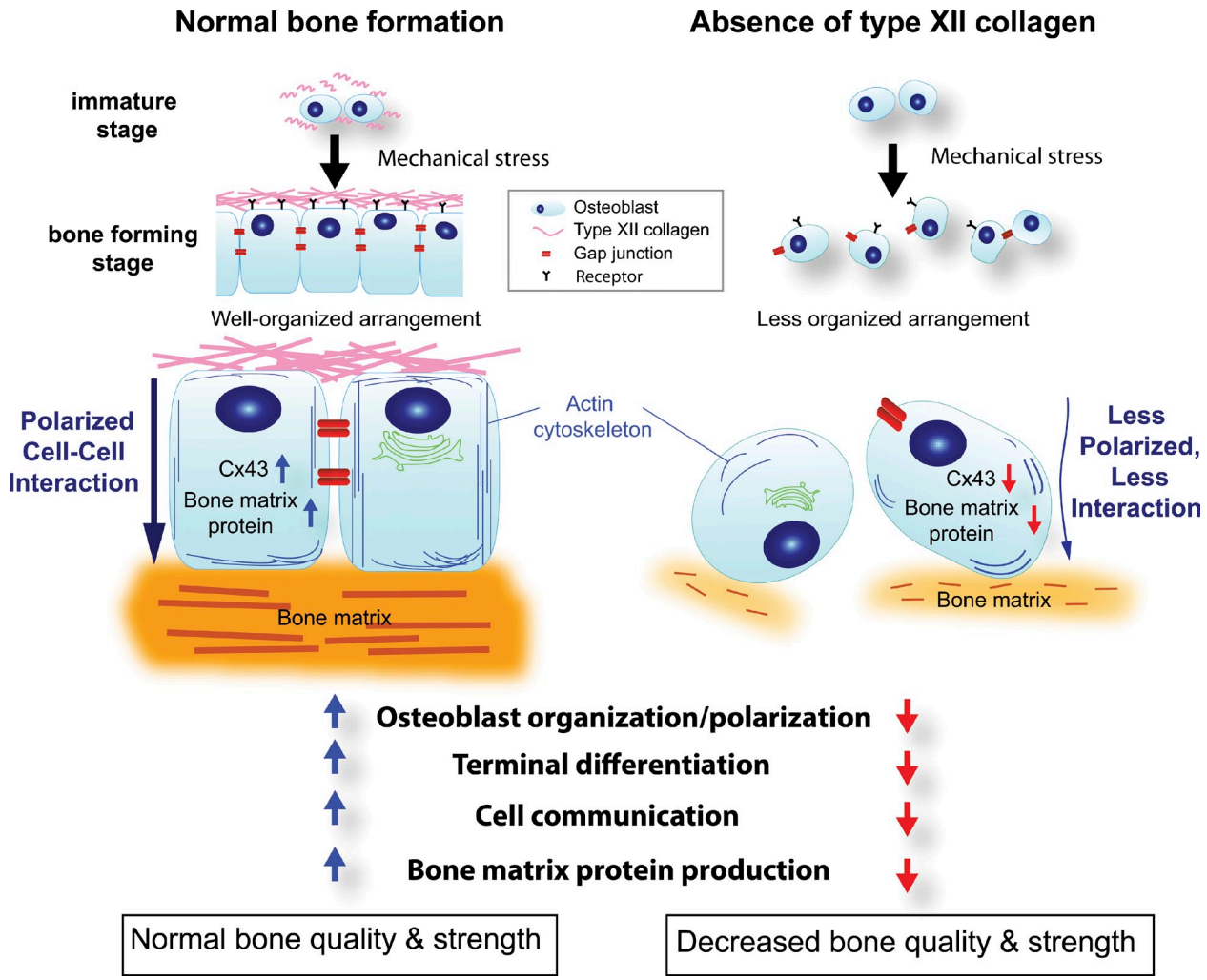

Figure 9. **Model for role of type XII collagen in osteoblast development and bone formation.** Type XII collagen surrounding immature osteoblasts responds to mechanical stimuli that initiate osteoblast maturation. This is associated with increased osteoblast organization, cell–cell interaction, and polarization along bone deposition interfaces. Further localized production of type XII collagen by well-organized polar osteoblasts reinforces the osteoblast organization and maturation. Cell–cell interaction drives Cx43 expression, thereby establishing cell communication via gap junctions, resulting in terminal differentiation, increased bone matrix protein production, and organized deposition of a functional bone matrix. In the absence of type XII collagen, there is a dysfunctional response to the mechanical stimuli and an alteration in the osteoblast maturation sequence. This defect delays/alters osteoblast organization, polarity, and cell–cell contacts, and, therefore, the downstream pathways, including up-regulation of Cx43 and bone matrix proteins, are compromised. Together, this results in decreased bone formation and quality.

in osteoporosis, bone fracture healing, and bone implantation. Bone matrix mainly consists of type I collagen. Collagen fibrils regulate mineral deposition and growth (Murshed et al., 2005). FACIT collagens, including type XII collagen, play a role in collagen fibril formation by providing specific molecular bridges between fibrils and other matrix components (Gordon and Olsen, 1990; van der Rest and Garrone, 1991; Gordon and Hahn, 2010; Birk and Brückner, 2011). In this study, although the expression of type I collagen did not change, the absence of type XII collagen decreased bone matrix proteins such as osteocalcin and osteopontin. A recent study demonstrated that osteopontin regulates bone toughness by mediating matrix heterogeneity in bone matrix (Thurner et al., 2010). This supports a role for fibril-associated type XII collagen in modification of collagen fibril properties, resulting in the regulation of bone matrix formation and mineralization. Type XII collagen may provide a target to develop treatment modalities for bone fracture healing and transplantation.

In conclusion, we propose a model in which type XII collagen is involved in the regulation of bone formation (Fig. 9). Type XII collagen surrounding immature osteoblasts, either alone or as a complex, responds to mechanical stimuli that initiate osteoblast maturation. This is associated with increased type XII collagen synthesis and secretion as well as localized deposition of type XII collagen along the maturing osteoblast boundary. This results in well-organized polarized osteoblasts driving osteoblast organization, cell–cell interaction, and maturation. Osteoblast organization, cell–cell interaction, and polarization along bone deposition interfaces drive Cx43 expression, thereby establishing gap junction–mediated cell communication resulting in terminal differentiation, increased bone matrix protein production, and organized deposition of a functional bone matrix. In contrast, when type XII collagen is absent, there is a dysfunctional response to the mechanical stimuli and an alteration in the osteoblast maturation sequence. This defect delays/alters

osteoblast organization, polarity, and cell–cell contacts, and, therefore, the downstream pathways are compromised, including up-regulation of Cx43 and bone matrix proteins. In addition, altered cell interactions result in an abnormal regulation of the osteoblast to osteocyte transition. Together, this results in decreased bone formation and altered quality. This is a novel finding indicating that type XII collagen in the extracellular matrix plays important roles in osteoblast development. Furthermore, determination of osteoblast shape, organization, and communication are crucial events in osteoblast terminal differentiation and the high quality production of bone matrix. Because type XII collagen is distributed in all the bone-forming areas, this regulation is crucial for general bone formation.

Materials and methods

Animals

Col12a1 knockout mice were generated on a mixed background with C57BL/6 and 129/SvJ. Homologous recombination was performed using a construct including neomycin-polyadenylation signal (poly A) under the control of phosphoglycerolkinase, which was inserted into exons 2–5 of the *Col12a1* gene and was not removed from the line studied. Mice were backcrossed into the C57BL/6 background and demonstrated increased perinatal lethality. To circumvent this, the line was bred with 129/SvJ mice and the offspring used for this work. Both mutant and control mice were in mixed C57BL/6-129/SvJ backgrounds. Mutant mice in both backgrounds had comparable phenotypes. Parameters defining the phenotype for the organism (i.e., body weight), bone function (i.e., biomechanical parameters including the maximum load to failure), and bone structure (i.e., fiber organization and amount) were examined in wild-type, heterozygous, and homozygous mice. There were no significant differences observed in these parameters between wild-type and heterozygous mice. All animal studies were performed in compliance with the Institutional Animal Care and Use Committee–approved protocols.

Whole mouse skeletal analysis

For x-ray analysis, 5-mo-old *Col12a*$^{+/+}$ and *Col12a1*$^{-/-}$ mice were anesthetized, and images were taken with an x-ray generator (Polymat 70; Siemens) using 44 kV and 6.4 mA. After x-ray analysis, whole mount mouse skeletal staining was performed as previously described (McLeod, 1980). In brief, the animals were sacrificed, skinned, eviscerated, and fixed in 96% ethanol for 48 h. The cartilage was stained with alcian blue (0.015% in 80% ethanol and 20% acetic acid) for 48 h followed by incubation in 96% ethanol for 3 d. Samples were cleared by immersion in 2% KOH overnight. Bones were counterstained with alizarin red for 5 h (50 mg/liter alizarin red in 1% KOH). After transfer of the stained skeletons to 2% KOH for 5 d to dissolve the soft tissue, the samples were preserved in 1% KOH and glycerol (20:80).

3D micro-CT analysis

Diaphyseal cross-sectional morphology and tissue mineral density (TMDn) of the femur were measured using an eXplore Locus SP Pre-Clinical Specimen micro-CT system (GE Healthcare) according to previously published methods (Jepsen et al., 2007). 3D images of the mid-diaphysis, which was located immediately distal to the third trochanter, were obtained at an 8.7-µm voxel size. The scan protocol consisted of 3,600 image acquisitions over a 5-h scan (acquisition parameters: 80 kVp, 80 µA, 3-s exposure time [~69 kJ], and 0.010 in. of aluminum beam filter). Femurs were individually thresholded (Otsu, 1979) to segment bone and nonbone voxels. Morphological traits describing the amount of tissue (cortical area, marrow area, total area, and cortical thickness) and the spatial distribution of tissue (moment of inertia, J) were quantified. Total bone area was defined as the sum of the cortical and marrow areas. The relative cortical area (cortical area/total area) provided a measure of the proportion of the total area that was occupied by bone. These traits were quantified for each cross section, and the values were averaged over the analysis region. TMDn, which is the mean mineral value of the bone voxels only expressed in hydroxyapatite (HA) density equivalents, was calculated by converting the grayscale output of bone voxels in Hounsfield units (HUs) to mineral values (milligrams/cubic centimeters of HA) through the use of a calibration phantom containing air, water, and HA (SB3; Gammex RMI). TMDn was defined as the mean bone voxel HU value divided by the mean of the HU value of the HA phantom multiplied by 1,130 mg/cm^3 (HA physical density). The same calibration phantom was included in all scans to adjust mineral density measurements for the variability in x-ray attenuation inherent to independent scan sessions (Jepsen et al., 2007).

Mechanical property analysis

After micro-CT analysis, femurs were loaded to failure in four-point bending at 0.05 mm/s to assess whole bone mechanical properties (Jepsen et al., 2003). Load deflection curves were analyzed for stiffness (the slope of the initial portion of the curve), maximum load, postyield deflection, and work to failure. Femurs were tested at RT and kept moist with PBS during all tests. Because body weight differed for *Col12a*$^{+/+}$ and *Col12a1*$^{-/-}$ mice, differences in mechanical properties were not only determined by comparing group means but also by testing whether the femurs were less stiff and less strong relative to body size (Jepsen et al., 2003). For the latter analysis, whole bone stiffness and maximum load were plotted against body weight, and the slopes and intercepts of linear regressions were compared by analysis of covariance.

Histomorphometric analysis

To analyze in vivo bone formation, calcein labeling was conducted to determine the levels of newly formed bone within a unit time period according to the methods previously described (Izu et al., 2009). In brief, calcein (10 mg/kg of body weight) was injected intraperitoneally 2 and 7 d before sacrifice. Femurs were fixed in 4% paraformaldehyde and rinsed in 0.1 M phosphate buffer. Femurs were embedded undecalcified in polymethylmethacrylate, and 40-µm-thick cross sections were prepared from the mid-diaphysis. The analysis site was standardized by examining the cross section located immediately distal to the third trochanter. The histomorphometric indices of osteoblastic activity included percentage of labeled perimeter (L.Pm/B.Pm,%), bone formation rate, and mineral apposition rate. The histomorphometric index of osteoclastic activity included percentage of eroded perimeter (Er.Pm/B.Pm,%). To analyze bone turnover, osteoclast number per bone surface (N.S/BS, N/mm) and osteoclast surface per bone surface (Oc.S/BS,%) were analyzed by TRAP staining of 5-µm cross sections of femurs as previously described (Izu et al., 2009).

Mineralized nodule analysis

Mineralized nodule assays were performed as previously described (Izu et al., 2009). Bone marrow cells were obtained from P30 *Col12a1*$^{+/+}$ (n = 5) and *Col12a1*$^{-/-}$ (n = 6) mice and seeded into 12-well plates (2.0 cm^2/well) at a density of 2 × 10^5 cells/well. The bone marrow cells were cultured in a standard growth medium containing 50 µg/ml ascorbic acid and 10 mM β-glycerophosphate. The medium was changed every 2 d. The cultures were harvested on days 14, 21, and 28 and stained with alizarin red solution. At each time point, cells from each individual mouse were analyzed in triplicate. The area of mineralized nodules/total dish was measured with the ImageJ Analysis Program (National Institutes of Health).

Bone resorption assay

RatLaps ELISA (Immunodiagnostic Systems) was used for bone resorption assay in vivo by quantitatively determining the C-terminal telopeptide α1 chain of type I collagen in mouse serum. Serum was obtained from wild-type mice (n = 4) and *Col12a1*$^{-/-}$ (n = 5) mice at P30 and analyzed in duplicate.

Histological examination

Femurs were dissected from wild-type and *Col12a1*$^{-/-}$ mice at P14 and P30 and fixed in 4% paraformaldehyde in 0.1 M phosphate buffer, pH 7.4, at 4°C overnight. The tissues were decalcified in 15% EDTA in 0.01 M phosphate buffer, pH 7.4, at 4°C for 1 wk and then embedded in an optimal cutting temperature compound, frozen by liquid nitrogen, and stored at −80°C. Cross sections were stained with H&E to observe bone histological phenotypes, with Sirius red to observe collagen arrangement under polarized microscopy, and with immunostaining to detect cell polarization under confocal microscopy. Osteocyte density was measured in H&E cross sections of P14 wild-type (n = 3) and type XII collagen–null (n = 3) mice. Five different areas per individual mice were randomly selected, and the numbers of osteocytes in cortical bone areas were calculated.

Immunolocalization analysis

Immunostaining was performed as previously described (Izu et al., 2009). In brief, 5-µm cross and longitudinal sections of the femur diaphysis from

P30 wild-type and *Col12a1*$^{-/-}$ mice were prepared. The cryosections were blocked by 5% goat serum and then were incubated with rabbit anti–type XII collagen antibodies (Veit et al., 2006) using a 1:1,000 dilution at 4°C overnight. The secondary antibody was Alexa Fluor 488 goat anti–rabbit IgG (Invitrogen) used at 1:500. Vectashield mounting solution with DAPI (Vector Laboratories) was used as a nuclear marker. Images were captured using a fluorescence microscope (DM5500; Leica). Identical conditions and set integration times were used to facilitate comparisons between samples. To investigate cell polarity, 10-µm cross sections of P30 *Col12a1*$^{+/+}$ and *Col12a1*$^{-/-}$ femur diaphysis were incubated with rabbit monoclonal anti-GM130 antibody (EP892Y; Abcam) using a 1:50 dilution. Alexa Fluor 555 goat anti–rabbit IgG (Invitrogen) and Alexa Fluor 488–phalloidin (Invitrogen) were used at 1:200. Images were captured using a confocal laser-scanning microscope (FV1000 MPE; Olympus) with a 60× 1.42 NA oil immersion lens. To avoid bleedthrough between fluorescence emissions, samples were scanned sequentially with 405-, 488-, and 543-nm lasers, and emissions were collected with appropriate spectral slit settings.

Transmission EM

Femur samples from *Col12a*$^{+/+}$ and *Col12a1*$^{-/-}$ mice at P14 were analyzed by transmission EM (Birk and Trelstad, 1984). In brief, femurs were dissected and fixed in 4% paraformaldehyde, 2.5% glutaraldehyde, and 0.1 M sodium cacodylate, pH 7.4, with 8.0 mM $CaCl_2$ at 4°C overnight and then decalcified in 15% EDTA in 0.01 M phosphate buffer, pH 7.4, at 4°C for 1 wk. The femurs were postfixed with 1% osmium tetroxide and dehydrated in an ethanol series followed by propylene oxide. The tissue samples were infiltrated and embedded in a mixture of EMbed 812, nadic methyl anhydride, dodecenylsuccinic anhydride, and DMP-30 (Electron Microscopy Sciences). 90-nm thin sections were cut using an ultramicrotome (UCT; Reichert) and poststained with 2% aqueous uranyl acetate and 1% phosphotungstic acid, pH 3.2. Cross sections from the midshafts of the femurs were examined at 80 kV using a transmission electron microscope (1400; JEOL) equipped with a digital camera (Orius; Gatan, Inc.).

Primary osteoblast culture

Primary mouse osteoblastic cells were obtained by sequential enzyme digestion of excised calvarial bones from neonatal mice using 2% dispase and 1% collagenase in PBS. The cells were resuspended in α-MEM (Invitrogen) supplemented with 10% FBS (Invitrogen) and 1% antibiotics (Invitrogen). Osteoblasts were initially seeded at a density of 2×10^5 cells/6-cm dish. At confluency, the culture medium was changed to the growth medium containing 50 µg/ml ascorbic acid and 10 mM β-glycerophosphate. The medium was changed every 2 d. The cells were collected on day 0, 7, 14, and 21 after changing to growth medium. The collected cells were used for the analysis of real-time PCR, Western blotting, and dye coupling assays.

Lentivirus shRNA production and transduction

Lentiviral constructs carrying shRNA-targeting mouse *Col12a1* were purchased from Thermo Fisher Scientific. Five mouse *Col12a1* shRNA clones (V2LMM_15532, V2LMM_17805, V3LMM_459147, V3LMM_459151, and V3LMM_459152) were screened. The nonsilencing GFP lentivirus was used as a control. Plasmid DNA was amplified and purified using a HiSpeed Plasmid Midi kit (QIAGEN) and then transfected along with packaging plasmid into HEK293T cells to generate lentiviruses by using the Trans-Lentiviral GIPZ packaging system (Thermo Fisher Scientific). The cells were refed with DME medium supplemented with 10% FBS and 1× antibiotic–antimycotic (Invitrogen) 24 h after infection. The culture supernatant was harvested 72 h after transfection. The supernatant-containing lentivirus was centrifuged or filtered and used to infect the mouse preosteoblast cell line MC3T3-E1 purchased from American Type Culture Collection. The MC3T3-E1 cells were cultured with α-MEM supplemented with 10% FBS and 1× antibiotic–antimycotic (Invitrogen) as well as 2 µg/ml puromycin to select target cells. After selection for 7 d, cells were analyzed for in vitro differentiation and dye coupling assay.

PCR analysis

Total RNA was isolated from primary osteoblasts obtained from neonatal mouse calvaria, lentivirus-treated MC3T3-E1 cells, and P30 mouse femurs by using an RNeasy Lipid Tissue Mini kit (QIAGEN) according to the manufacturer's protocol. Reverse transcription was performed using 1 µg of total RNA with random primers (High-Capacity cDNA Reverse Transcription kit; Applied Biosystems). Quantitative real-time PCR analysis was performed using StepOnePlus (Applied Biosystems). The reaction was performed in a 25-µl reaction mixture containing 200 nM cDNA samples, 50 nM of sense and antisense primers, and 12.5 µl SYBR green PCR Master Mix (Applied Biosystems). The primer sequences are shown in Table I. The PCR conditions were initially 95°C for 20 s followed by 40 cycles at 95°C for 3 s and 60°C for 30 s. The mRNA expression levels were normalized by calculating the ratios against *Gapdh* expression levels.

Immunoblotting analysis

Flexor digitorum longus, tibia, muscle, skin, and cornea were removed from P30 *Col12a1*$^{+/+}$ and *Col12a1*$^{-/-}$ mice, and primary osteoblastic cells obtained from neonatal calvaria described in the previous section were used for Western blotting analysis. The whole tissue and cell lysate preparation and immunoblot were performed as previously described (Izu et al., 2009) using rabbit anti–type XII collagen (1:1,000 dilution; KR33), rabbit anti-Cx43 (1:10,000 dilution; Sigma-Aldrich), rabbit anti–mouse collagen I (1:1,000 dilution; Millipore), rabbit anti-Cad11 (1:250 dilution; Invitrogen), rabbit anti–N-cadherin (1:1,000 dilution; Cell Signaling Technology), 0.1 µg/ml of goat anti–mouse osteopontin (R&D Systems), goat anti-osteocalcin (1:100 dilution; Santa Cruz Biotechnology, Inc.), mouse anti–β-actin (1:5,000 dilution; Millipore), and anti–mouse or anti–rabbit HRP-conjugated secondary antibodies (GE Healthcare).

Dye coupling

Dye coupling analysis was used as previously described (Lecanda et al., 2000) to assess cell to cell diffusion of negatively charged dyes. Primary osteoblasts and lentivirus-induced knockdown MC3T3-E1 cells were used. In brief, primary osteoblasts obtained from each genotype group were preloaded with calcein AM (BD) and Cell Tracker (Invitrogen) for 15 min and mobilized by trypsin digestion and then were added on top of a monolayer of each cell type. Cell trace calcein red-orange AM (Invitrogen) was used for lentivirus-treated cells because cells were transduced *shGFP*. The "parachuted" cells were allowed to settle onto the unlabeled monolayer and returned to the incubator for 1 h. Because calcein dye is able to transfer through gap junctions but Cell Tracker remains in the plasma membrane, the transfer of calcein dye from donor to acceptor cells (host cells) was detected using a confocal laser-scanning microscope (SP2 DM IRE2; Leica). The images were taken with a 40× 1.25 NA oil immersion lens. Calcein AM and calcein red-orange AM signals from cells were collected with 488- and 561-nm lasers and appropriate spectral slit settings. Six different experimental groups were established, donor and host cells were either wild-type or *Col12a1*$^{-/-}$ cells, and donor cells of each genotype were seeded onto plates with no host cell as a control. The number of dye-transferred cells per total parachuted cells was determined in 10 random images acquired from each well (24-well plate), and 6 wells were used per experimental group. Images were captured using a spinning disk confocal system (Ultraview Vox; PerkinElmer) attached to an inverted microscope (Ti; Nikon). The images were taken with a 40× 1.3 NA oil immersion lens and an electron-multiplying charge-coupled device camera (C9100-13; Hamamatsu Photonics) using Velocity version 5.3.2 software. Calcein AM and Cell Tracker were excited with 488- and 561-nm laser lines, and emissions were collected with 527/55- and 587/125-nm band pass filters, respectively. Cells were maintained in α-MEM supplemented with 10% FBS and 1× antibiotic–antimycotic at 37°C during image capture.

Statistical analysis

Statistics were conducted as Student's *t* tests unless noted otherwise. Asterisks indicate $P < 0.05$, and double asterisks indicate $P < 0.01$. All of the numeral data in the results were presented as means ± SD.

Online supplemental material

Fig. S1 shows that altered bone matrix deposition observed in type XII collagen–null mice is not the result of altered bone resorption. Fig. S2 shows delayed terminal differentiation in type XII collagen knockdown MC3T3-E1 cells comparable with that seen in the type XII collagen–null mouse model. Fig. S3 shows increased osteocyte density in type XII collagen–null cortical bone, indicating dysfunctional regulation of osteoblast to osteocyte transition. Fig. S4 shows no alteration in Cad2 and Cad11 expression in the absence of type XII collagen in osteoblasts. Fig. S5 shows impaired gap junction function in *Col12a1* gene knockdown MC3T3-E1 cells comparable with that seen in the type XII collagen–null mice. Video 1 shows normal gap junction communication in *Col12a1*$^{+/+}$ osteoblasts, and Video 2 shows impaired gap junction communication in *Col12a1*$^{-/-}$ osteoblasts. Online supplemental material is available at http://www.jcb.org/cgi/content/full/jcb.201010010/DC1.

Table I. **Primer sets for real-time PCR**

Gene	Forward/reverse	Primer sequence
Col12a1	Forward	5′-ACCCACCTTCCGACTTGAATT-3′
	Reverse	5′-TAGGCCCATCTGTTGTAGGG-3′
Runx2	Forward	5′-CCCAGCCACCTTTACCTACA-3′
	Reverse	5′-TATGGAGTGCTGCTGGTCTG-3′
Ocn	Forward	5′-AAGCAGGAGGGCAATAAGGT-3′
	Reverse	5′-TAGGCGGTCTTCAAGCCATA-3′
Opn	Forward	5′-TGGTGCCTGACCCATCTCA-3′
	Reverse	5′-TCTTCAGAGGACACAGCATTCTG-3′
Cx43	Forward	5′-GTGGCCTGCTGAGAACCTAC-3′
	Reverse	5′-CTTGGCCCAGCCTCGAT-3′
Cad2	Forward	5′-CTGGGACGTATGTGATGACG-3′
	Reverse	5′-TGATGATGTCCCCAGTCTCA-3′
Cad11	Forward	5′-CACAGGATGGTGTGGTGAAG-3′
	Reverse	5′-AGGCTCATCGGCATCTTCTA-3′
Trap	Forward	5′-CAGAGTGGCTGTTGACTCCA-3′
	Reverse	5′-ACCAGCGCTTGGAGATCTTA-3′
Nfatc1	Forward	5′-GCACATTTGAGTCCGTGATG-3′
	Reverse	5′-GCAGAGCAAATGACTGTGGA-3′
Rank	Forward	5′-GCTGGCTACCACTGGAACTC-3′
	Reverse	5′-GTGCAGTTGGTCCAAGGTTT-3′
Rankl	Forward	5′-ACCAGCATCAAAATCCCAAG-3′
	Reverse	5′-AAGGGTTGGACACCTGGATG-3′
Gapdh	Forward	5′-TCAACAGCAACTCCCACTCTTCCA-3′
	Reverse	5′-ACCCTGTTGCTGTAGCCGTATTCA-3′

We thank Sheila M. Adams and Amanda Garces for technical assistance with the EM and Chinda Hemmavanh and Semra Oezcelik for their valuable technical assistance in the laboratory. We thank Dr. Marian F. Young for many helpful discussions.

This work was supported by grants from the National Institutes of Health (DEB AR44745, EY05129, KJJ AR44927, and AR056639).

Submitted: 4 October 2010
Accepted: 12 May 2011

References

Arai, K., Y. Nagashima, T. Takemoto, and T. Nishiyama. 2008. Mechanical strain increases expression of type XII collagen in murine osteoblastic MC3T3-E1 cells. *Cell Struct. Funct.* 33:203–210. doi:10.1247/csf.08025

Bader, H.L., D.R. Keene, B. Charvet, G. Veit, W. Driever, M. Koch, and F. Ruggiero. 2009. Zebrafish collagen XII is present in embryonic connective tissue sheaths (fascia) and basement membranes. *Matrix Biol.* 28:32–43. doi:10.1016/j.matbio.2008.09.580

Berthiaume, F., P.V. Moghe, M. Toner, and M.L. Yarmush. 1996. Effect of extracellular matrix topology on cell structure, function, and physiological responsiveness: hepatocytes cultured in a sandwich configuration. *FASEB J.* 10:1471–1484.

Birk, D.E., and P. Brückner. 2011. Collagens, suprastructures and collagen fibril assembly. *In* The Extracellular Matrix: an Overview. R.P. Mecham, editor. Springer, NY. 77–115.

Birk, D.E., and R.L. Trelstad. 1984. Extracellular compartments in matrix morphogenesis: collagen fibril, bundle, and lamellar formation by corneal fibroblasts. *J. Cell Biol.* 99:2024–2033. doi:10.1083/jcb.99.6.2024

Böhme, K., Y. Li, P.S. Oh, and B.R. Olsen. 1995. Primary structure of the long and short splice variants of mouse collagen XII and their tissue-specific expression during embryonic development. *Dev. Dyn.* 204:432–445. doi:10.1002/aja.1002040409

Burgstaller, G., M. Gregor, L. Winter, and G. Wiche. 2010. Keeping the vimentin network under control: cell-matrix adhesion-associated plectin 1f affects cell shape and polarity of fibroblasts. *Mol. Biol. Cell*. 21:3362–3375. doi:10.1091/mbc.E10-02-0094

Chiquet, M., U. Mumenthaler, M. Wittwer, W. Jin, and M. Koch. 1998. The chick and human collagen alpha1(XII) gene promoter—activity of highly conserved regions around the first exon and in the first intron. *Eur. J. Biochem.* 257:362–371. doi:10.1046/j.1432-1327.1998.2570362.x

Civitelli, R. 2008. Connexin43 modulation of osteoblast/osteocyte apoptosis: a potential therapeutic target? *J. Bone Miner. Res.* 23:1709–1711. doi:10.1359/jbmr.0811c

Denhardt, D.T., E.H. Burger, C. Kazanecki, S. Krishna, C.M. Semeins, and J. Klein-Nulend. 2001. Osteopontin-deficient bone cells are defective in their ability to produce NO in response to pulsatile fluid flow. *Biochem. Biophys. Res. Commun.* 288:448–453. doi:10.1006/bbrc.2001.5780

Dobrowolski, R., P. Sasse, J.W. Schrickel, M. Watkins, J.S. Kim, M. Rackauskas, C. Troatz, A. Ghanem, K. Tiemann, J. Degen, et al. 2008. The conditional connexin43G138R mouse mutant represents a new model of hereditary oculodentodigital dysplasia in humans. *Hum. Mol. Genet.* 17:539–554. doi:10.1093/hmg/ddm329

Duncan, R.L., and C.H. Turner. 1995. Mechanotransduction and the functional response of bone to mechanical strain. *Calcif. Tissue Int.* 57:344–358. doi:10.1007/BF00302070

Flück, M., M.N. Giraud, V. Tunç, and M. Chiquet. 2003. Tensile stress-dependent collagen XII and fibronectin production by fibroblasts requires separate pathways. *Biochim. Biophys. Acta*. 1593:239–248. doi:10.1016/S0167-4889(02)00394-4

Geiger, B., A. Bershadsky, R. Pankov, and K.M. Yamada. 2001. Transmembrane crosstalk between the extracellular matrix—cytoskeleton crosstalk. *Nat. Rev. Mol. Cell Biol.* 2:793–805. doi:10.1038/35099066

Globus, R.K., S.B. Doty, J.C. Lull, E. Holmuhamedov, M.J. Humphries, and C.H. Damsky. 1998. Fibronectin is a survival factor for differentiated osteoblasts. *J. Cell Sci.* 111:1385–1393.

Gordon, M.K., and R.A. Hahn. 2010. Collagens. *Cell Tissue Res.* 339:247–257. doi:10.1007/s00441-009-0844-4

Gordon, M.K., and B.R. Olsen. 1990. The contribution of collagenous proteins to tissue-specific matrix assemblies. *Curr. Opin. Cell Biol.* 2:833–838. doi:10.1016/0955-0674(90)90080-X

Grimston, S.K., M.D. Brodt, M.J. Silva, and R. Civitelli. 2008. Attenuated response to in vivo mechanical loading in mice with conditional osteoblast ablation of the connexin43 gene (Gja1). *J. Bone Miner. Res.* 23:879–886. doi:10.1359/jbmr.080222

Harada, S., and G.A. Rodan. 2003. Control of osteoblast function and regulation of bone mass. *Nature*. 423:349–355. doi:10.1038/nature01660

Ilvesaro, J., K. Metsikkö, K. Väänänen, and J. Tuukkanen. 1999. Polarity of osteoblasts and osteoblast-like UMR-108 cells. *J. Bone Miner. Res.* 14:1338–1344. doi:10.1359/jbmr.1999.14.8.1338

Imai, S., M. Kaksonen, E. Raulo, T. Kinnunen, C. Fages, X. Meng, M. Lakso, and H. Rauvala. 1998. Osteoblast recruitment and bone formation enhanced by cell matrix-associated heparin-binding growth-associated molecule (HB-GAM). *J. Cell Biol.* 143:1113–1128. doi:10.1083/jcb.143.4.1113

Imbeault, S., L.G. Gauvin, H.D. Toeg, A. Pettit, C.D. Sorbara, L. Migahed, R. DesRoches, A.S. Menzies, K. Nishii, D.L. Paul, et al. 2009. The extracellular matrix controls gap junction protein expression and function in postnatal hippocampal neural progenitor cells. *BMC Neurosci.* 10:13. doi:10.1186/1471-2202-10-13

Izu, Y., F. Mizoguchi, A. Kawamata, T. Hayata, T. Nakamoto, K. Nakashima, T. Inagami, Y. Ezura, and M. Noda. 2009. Angiotensin II type 2 receptor blockade increases bone mass. *J. Biol. Chem.* 284:4857–4864. doi:10.1074/jbc.M807610200

Jepsen, K.J., O.J. Akkus, R.J. Majeska, and J.H. Nadeau. 2003. Hierarchical relationship between bone traits and mechanical properties in inbred mice. *Mamm. Genome*. 14:97–104. doi:10.1007/s00335-002-3045-y

Jepsen, K.J., B. Hu, S.M. Tommasini, H.W. Courtland, C. Price, C.J. Terranova, and J.H. Nadeau. 2007. Genetic randomization reveals functional relationships among morphologic and tissue-quality traits that contribute to bone strength and fragility. *Mamm. Genome*. 18:492–507. doi:10.1007/s00335-007-9017-5

Jiang, J.X., A.J. Siller-Jackson, and S. Burra. 2007. Roles of gap junctions and hemichannels in bone cell functions and in signal transmission of mechanical stress. *Front. Biosci.* 12:1450–1462. doi:10.2741/2159

Jin, X., S. Iwasa, K. Okada, A. Ooi, K. Mitsui, and M. Mitsumata. 2003. Shear stress-induced collagen XII expression is associated with atherogenesis. *Biochem. Biophys. Res. Commun.* 308:152–158. doi:10.1016/S0006-291X(03)01344-5

Kim, S.H., J.E. Turnbull, and S.E. Guimond. 2011. Extracellular matrix and cell signalling: the dynamic cooperation of integrin, proteoglycan and growth factor receptor. *J. Endocrinol.* 209:139–151. doi:10.1530/JOE-10-0377

Koga, T., Y. Matsui, M. Asagiri, T. Kodama, B. de Crombrugghe, K. Nakashima, and H. Takayanagi. 2005. NFAT and Osterix cooperatively regulate bone formation. *Nat. Med.* 11:880–885. doi:10.1038/nm1270

Komori, T. 2010. Regulation of osteoblast differentiation by runx2. *Adv. Exp. Med. Biol.* 658:43–49. doi:10.1007/978-1-4419-1050-9_5

Lecanda, F., P.M. Warlow, S. Sheikh, F. Furlan, T.H. Steinberg, and R. Civitelli. 2000. Connexin43 deficiency causes delayed ossification, craniofacial abnormalities, and osteoblast dysfunction. *J. Cell Biol.* 151:931–944. doi:10.1083/jcb.151.4.931

Matsuo, K., and N. Irie. 2008. Osteoclast-osteoblast communication. *Arch. Biochem. Biophys.* 473:201–209. doi:10.1016/j.abb.2008.03.027

McLeod, M.J. 1980. Differential staining of cartilage and bone in whole mouse fetuses by alcian blue and alizarin red S. *Teratology*. 22:299–301. doi:10.1002/tera.1420220306

Murshed, M., D. Harmey, J.L. Millán, M.D. McKee, and G. Karsenty. 2005. Unique coexpression in osteoblasts of broadly expressed genes accounts for the spatial restriction of ECM mineralization to bone. *Genes Dev.* 19:1093–1104. doi:10.1101/gad.1276205

Nakashima, K., X. Zhou, G. Kunkel, Z. Zhang, J.M. Deng, R.R. Behringer, and B. de Crombrugghe. 2002. The novel zinc finger-containing transcription factor osterix is required for osteoblast differentiation and bone formation. *Cell*. 108:17–29. doi:10.1016/S0092-8674(01)00622-5

Nishiyama, T., A.M. McDonough, R.R. Bruns, and R.E. Burgeson. 1994. Type XII and XIV collagens mediate interactions between banded collagen fibers in vitro and may modulate extracellular matrix deformability. *J. Biol. Chem.* 269:28193–28199.

Oh, S.P., R.W. Taylor, D.R. Gerecke, J.M. Rochelle, M.F. Seldin, and B.R. Olsen. 1992. The mouse alpha 1(XII) and human alpha 1(XII)-like collagen genes are localized on mouse chromosome 9 and human chromosome 6. *Genomics*. 14:225–231. doi:10.1016/S0888-7543(05)80210-1

Otsu, N. 1979. A threshold selection method from gray-level histograms. *IEEE Trans. Syst. Man Cybern.* SMC-9:62–66.

Parsons, J.T., A.R. Horwitz, and M.A. Schwartz. 2010. Cell adhesion: integrating cytoskeletal dynamics and cellular tension. *Nat. Rev. Mol. Cell Biol.* 11:633–643. doi:10.1038/nrm2957

Rozario, T., and D.W. DeSimone. 2010. The extracellular matrix in development and morphogenesis: a dynamic view. *Dev. Biol.* 341:126–140. doi:10.1016/j.ydbio.2009.10.026

Shapiro, F. 2008. Bone development and its relation to fracture repair. The role of mesenchymal osteoblasts and surface osteoblasts. *Eur. Cell. Mater.* 15:53–76.

Stains, J.P., J.A. Weber, and C.V. Gay. 2002. Expression of Na(+)/Ca(2+) exchanger isoforms (NCX1 and NCX3) and plasma membrane Ca(2+) ATPase during osteoblast differentiation. *J. Cell. Biochem.* 84:625–635. doi:10.1002/jcb.10050

Théry, M., V. Racine, A. Pépin, M. Piel, Y. Chen, J.B. Sibarita, and M. Bornens. 2005. The extracellular matrix guides the orientation of the cell division axis. *Nat. Cell Biol.* 7:947–953. doi:10.1038/ncb1307

Thurner, P.J., C.G. Chen, S. Ionova-Martin, L. Sun, A. Harman, A. Porter, J.W. Ager III, R.O. Ritchie, and T. Alliston. 2010. Osteopontin deficiency increases bone fragility but preserves bone mass. *Bone*. 46:1564–1573. doi:10.1016/j.bone.2010.02.014

van der Rest, M., and R. Garrone. 1991. Collagen family of proteins. *FASEB J.* 5:2814–2823.

Veit, G., U. Hansen, D.R. Keene, P. Bruckner, R. Chiquet-Ehrismann, M. Chiquet, and M. Koch. 2006. Collagen XII interacts with avian tenascin-X through its NC3 domain. *J. Biol. Chem.* 281:27461–27470. doi:10.1074/jbc.M603147200

Wessel, H., S. Anderson, D. Fite, E. Halvas, J. Hempel, and N. SundarRaj. 1997. Type XII collagen contributes to diversities in human corneal and limbal extracellular matrices. *Invest. Ophthalmol. Vis. Sci.* 38:2408–2422.

Yoshida, C.A., T. Furuichi, T. Fujita, R. Fukuyama, N. Kanatani, S. Kobayashi, M. Satake, K. Takada, and T. Komori. 2002. Core-binding factor beta interacts with Runx2 and is required for skeletal development. *Nat. Genet.* 32:633–638. doi:10.1038/ng1015

Zimmerman, D., F. Jin, P. Leboy, S. Hardy, and C. Damsky. 2000. Impaired bone formation in transgenic mice resulting from altered integrin function in osteoblasts. *Dev. Biol.* 220:2–15. doi:10.1006/dbio.2000.9633